LATTICE MODELS FOR THE PREDICTION OF LOAD-INDUCED FAILURE AND DAMAGE IN WOOD

William G. Davids
Assistant Professor

Eric N. Landis
Associate Professor

and

Svetlana Vasic†
Post-doctoral Research Associate
Department of Civil and Environmental Engineering
University of Maine
Orono, ME 04469-5711

(Received January 2002)

ABSTRACT

Lattice models, which are essentially networks of springs having variable strength and stiffness, are used to predict the response of structural softwood to various mechanical loadings. The use of lattice models is motivated by the desire to mimic the morphology of wood, and thus realistically predict both load-displacement response and experimentally observed damage patterns that are not well captured by conventional continuum-based models. The goal of the work described in this paper was to evaluate suitability of lattice models for predicting several different failure modes of structural softwood, and to establish a methodology for matching model parameters to measured material properties. Using least squares techniques, the lattice model member properties were determined to give optimal predictions of bulk elastic constants and expected load-displacement response to failure under perpendicular-to-grain tension, parallel-to-grain tension, and shear. The lattice models were shown to accurately capture load-displacement response, including experimentally observed strain softening under perpendicular-to-grain tension. In addition, the lattice models successfully predicted damage localization, including crack bridging and microcracking around the critical crack. Mesh size effects were also examined, and while the lattice models are dependent on mesh size, it is demonstrated that for a fixed cell aspect ratio, a simple scaling of the lattice model strength and stiffness properties to account for cell size can yield reasonable predictions of ultimate capacity.

Keywords: Strain softening, lattice models, crack bridging, fracture, finite element analysis.

INTRODUCTION

The heterogeneous nature of wood and wood composites has presented scientists and engineers with a difficult modeling problem for many years. In the context of mechanical properties, continuum-based strength of materials approaches have been the primary methods for modeling the response of materials and structures to loads. For elastic and viscoelastic deformations, anisotropic continuum theory is an effective tool for predicting structural response. However, for prediction of element strength or structural load capacity, the effectiveness of traditional elasticity theory or a strength of materials approach can be called into question. This is especially true for a material that has substantial defects, or a material that has been subject to various degrees of damage. Indeed, typical coefficients of variation (COVs) for strength properties of wood are in the range of 14 to 28% (Wood Handbook 1999), whereas a typical COV for yield

† Member of SWST.

Wood and Fiber Science, 35(1), 2003, pp. 120–134

strength of structural steel is around 2% (Illston 1994).

The wide range of COVs observed in wood arises from the heterogeneous nature of the material and the statistical variations in local properties that arise from it. Wood is particularly difficult to model because the heterogeneities cover a wide range of length scales. Property variations are influenced by macroscopic heterogeneities such as knots, grain angle deviations, and the differing characteristics of earlywood and latewood, as well as microscopic heterogeneities such as variations in microfibril angle. Traditional mechanics of materials assumes that the influence of these local property variations are evenly distributed over the volume of the material. While this assumption is reasonably valid for predicting yield of ductile metals, for wood it is not. Local property variations in wood dictate the strength, and the wide range of relevant length scales does not validate spatial leveling up of local properties.

The typically nonductile fracture of wood observed in tension and shear has led researchers to investigate the role of cracks on strength. For example, Cramer and Goodman (1983) proposed the concept that tensile failure of a solid wood board arises from progressive fracture, and later developed a sophisticated finite-element model of a board that incorporated knots, grain pattern, and fracture mechanics to predict failure (Cramer and Goodman 1986). Cramer and Fohrell (1990) subsequently extended this model to capture progressive and mixed-mode fracture. These studies were valuable in that they recognized and attempted to rationally incorporate observed behavior and heterogeneities. However, the continuum framework implicit in these models ultimately limits their applicability.

The work described in this paper represents a different approach for modeling heterogeneous material behavior. Specifically, we develop a lattice finite element model where the lattice elements represent specific microstructural elements. While lattice models have been identified as a natural choice for modeling disordered materials due to the relative ease of explicitly incorporating heterogeneity and variability (Curtin and Scher 1990; Jirásek and Bažant 1995; Schlangen and Garboczi 1996, 1997), their ability to mimic the structure of an ordered, anisotropic, defect-sensitive material makes them an attractive candidate for modeling wood. Such a "morphology-based" model has several advantages over traditional continuum representations. First, the model can represent the material in a way that has a physical basis. The model elements are arranged in a lattice that mimics the material structure. Effects of local variations in fiber orientation, defects, and other heterogeneities can be incorporated directly into the model. Second, the changes in microstructural features that arise from damage-inducing mechanisms can be handled explicitly through broken elements. Third, and most significant, the modeling approach allows the macroscopic behavior of the material to be computationally linked to the micro- and meso-level features (such as grain angle deviations and knots) that cause that behavior. Damage, defects, and other microstructural features can be quantitatively linked to changes in material stiffness and strength. The result is a model that predicts *both* load-deformation response *and* microstructural damage patterns and failure modes.

The goal of the work described in this paper is to evaluate the suitability of lattice models for predicting different common failure modes of structural softwood. After an overview of the modeling approach, we first demonstrate how to adjust lattice properties to mimic bulk elastic properties under various loading conditions. Following this, a typical lattice model is calibrated to replicate the load-displacement response of eastern spruce loaded to failure under perpendicular-to-grain tension, parallel-to-grain tension, and shear. Model-predicted progressive fracture patterns are presented, and the effect of mesh size on model response is addressed. The potential for the practical application of lattice models is also discussed, with attention given to the explicit consider-

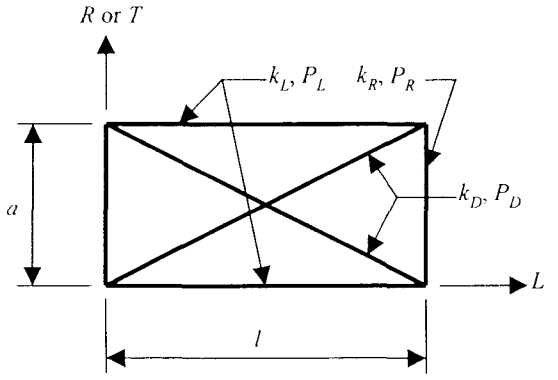

FIG. 1. Lattice cell geometry and member definitions.

ation of macrostructural defects and the issue of computational requirements.

DETAILS OF LATTICE MODEL

The 2D model detailed in this paper treats wood as a lattice composed of fiber bundles oriented in the longitudinal direction (denoted by *L*), ties between fibers oriented perpendicular-to-grain (*R* or *T* direction), and diagonal members (denoted by *D*) that are primarily responsible for transferring in-plane shear between adjacent fiber bundles. All members are treated as pinned-end bar elements, carrying only axial load. Each member in the lattice has a characteristic strength, *P* [N] and stiffness, *k* [N/mm]. Figure 1 illustrates the basic configuration of a single model cell having a length *l* and height *a*, and Fig. 2 shows three different finite element meshes of a small piece of clear-grained wood that is composed of an array of the individual cells.

An additional parameter not shown in Fig. 1 is the orientation of the diagonal, *D*, relative to *L*. We note that in a conventional stiffness-based structural analysis, the orientation θ is computed from the orientation of the element in the global coordinate system (i.e., $\theta = \tan^{-1}(a/l)$). However, our preliminary simulations showed that if θ is computed from the true lattice geometry, it is not possible to achieve a good prediction of the elastic constants with the lattice model. Therefore, θ was kept as an independent model parameter that

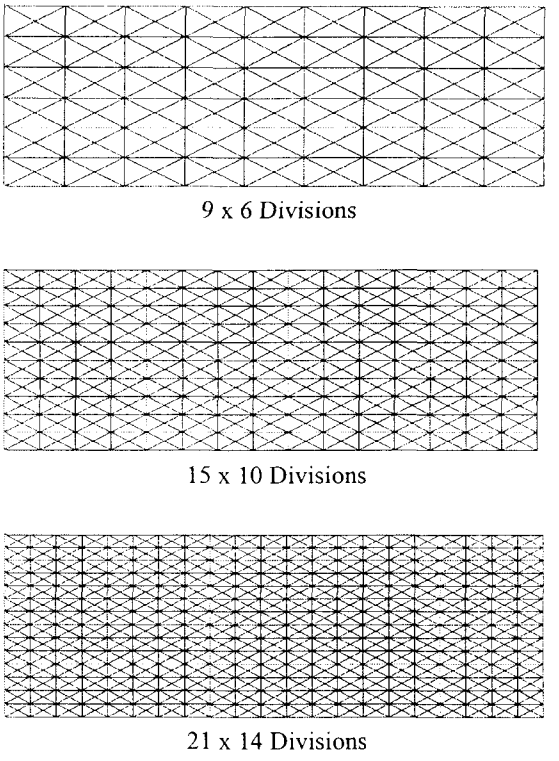

FIG. 2. Lattice models with varying levels of refinement.

did not depend on the cell aspect ratio, which allowed the relative contribution of the diagonal members to perpendicular-to-grain tension and in-plane shear to be adjusted independently of the cell geometry. The element stiffness matrices, element nodal force vectors, and element nodal displacements were transformed with this independent value of θ, which ensured that equilibrium and compatibility were always satisfied in the analysis.

The strength and stiffness values for each member are taken as random variables that obey a given probability distribution. This statistical distribution of member strengths within a specimen gives rise to the progressive and dispersed damage commonly observed in wood specimens loaded to failure under simple stress states (Vasic and Smith 1996; Vasic 2000; Vasic et al. 2001). Currently, the form of the distribution of lattice member strengths and stiffness is unknown, and a normal distri-

bution is assumed. Tensile and compressive strengths are considered equal in the present formulation, although the model can easily be extended to incorporate different member strengths in tension and compression. No attempt is made here to model variations in strength due to macrostructural features such as earlywood/latewood boundaries, although this issue is discussed later in this paper. Figure 3 shows the assumed brittle load-displacement relationship for each lattice member.

The foregoing model description leads to a solution procedure based on a stiffness-based matrix formulation for trusses and frames, which yields the following system of coupled linear equations at every load step:

$$\mathbf{KU} = \mathbf{F} \tag{1}$$

In Eq. (1), **K** is the system stiffness matrix, which is assembled from the individual element stiffness matrices, **U** is the vector of unknown nodal displacements, and **F** is a vector of known forces. For details of the stiffness method for trusses and frames, see a text on structural analysis such as Au and Christiano (1993) or Hibbeler (1990). We have chosen to employ a straightforward solution algorithm that relies on checking for failed elements at each load increment, and then removing the failed elements from the model and re-solving the system stiffness equations. While this approach has been adopted by most prior researchers who have used lattice models to capture failure and fracture in concrete (Raghuprasad et al. 1998; Schlangen and Garboczi 1996), we do note that more sophisticated algorithms can be employed that could save significant computation expense for large 3D simulations (Jirásek and Bažant 1995). The solution algorithm is given below for N load increments; the number of members failed within each load increment is denoted by n_f. The algorithm and all necessary routines required to assemble **K** and compute member forces have been implemented with the scientific computing package Matlab ("Using Matlab" 1998).

```
generate k and P for all members
assemble K
for i = 1 . . . N
  do
    form F
    U = K^-1 F
    compute forces in individual members
    compute n_f
    remove failed members from K
  while n_f > 0
end for
```

ALGORITHM 1. Solution of lattice model with progressive failure.

ESTIMATION OF MEAN STIFFNESS PARAMETERS

The first challenge in the application of the proposed lattice model for wood is to determine the member properties so that the well-known orthotropic elastic constants can be accurately predicted. With reference to Fig. 1, there are essentially two geometric parameters that can be adjusted: the aspect ratio l/a, which governs the relative number of L-direction, R-direction, and diagonal elements within a given model, and θ. For a 2D model in the LR plane such as that shown in Fig. 1, the mean stiffness of each member type ($\bar{k}_L$, $\bar{k}_R$, and $\bar{k}_D$) is a model parameter. The four elastic constants that must be matched by adjusting these model parameters are the elastic moduli E_L and E_R, the shear modulus G_{LR}, and Poisson's ratio ν_{LR}. Note that ν_{RL} is not considered, as it is very difficult to measure experimentally and its value is typically negligible (Bodig and Jayne 1993).

For the present simulation, model parameters were determined for a specimen with an overall length in the L-direction of 12 mm, a height in the R-direction of 4 mm, and a thickness of 12 mm. These dimensions are typical for the small-specimen tensile tests conducted on eastern Canadian spruce by Vasic (2000). To study the effect of model refinement, three levels of discretization ($L \times R$) were employed with the cell aspect ratio of $l/a = 2.0$: 9×6 divisions, 15×10 divisions, and 21×14 divisions, leaving only four independent model parameters. These three finite element meshes are shown in Fig. 2.

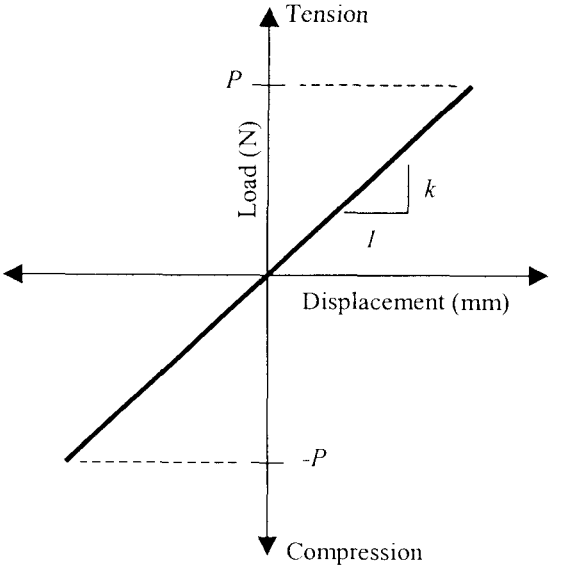

FIG. 3. Typical lattice element load-displacement relationship.

The modulus of elasticity E_R was taken as 519 MPa, which is the average secant modulus computed at a stress of approximately 0.3 MPa from the small specimen test data reported by Vasic (2000). This value is 37.5% less than the value of 830 MPa reported by Bodig and Goodman (1973) for red spruce (a species of spruce common to eastern Canada). To account for this observed difference in modulus, target values for the remaining elastic moduli were taken from the Wood Handbook (1999) for red spruce and reduced by 37.5%, giving E_L = 7,200 MPa and G_{LR} = 437 MPa. The value of ν_{LR} (Poisson's ratio) was taken to be 0.40, which is typical for spruce. Optimal values for the four independent model parameters were determined by minimizing the following least-squares objective function, Φ_S, which is normalized to give equal weight to all elastic constants:

$$\Phi_S(\theta, k_L, k_R, k_D) = \left[\left(\frac{(E_R - E_R^*)}{E_R}\right)^2 + \left(\frac{(E_L - E_L^*)}{E_L}\right)^2 + \left(\frac{(G_{LR} - G_{LR}^*)}{G_{LR}}\right)^2 + \left(\frac{(\nu_{LR} - \nu_{LR}^*)}{\nu_{LR}}\right)^2\right]^{1/2} \quad (2)$$

In Eq. (2), E_L^*, E_R^*, G_{LR}^*, and ν_{LR}^* are the values predicted by the lattice model assuming linearly elastic response to the simple stress states of parallel-to-grain tension, radial tension perpendicular-to-grain, and in-plane shear parallel-to-grain. For all of the models, a strain of 0.1% was assumed in the simulations, and no members were allowed to fail.

The loading for the three stress states was applied by enforcing the displacements Δ_R, Δ_L, and Δ_{LR} at the model boundaries as shown in Fig. 4. For the case of radial tension perpendicular-to-grain, this simulates the displacement control used in the actual experiments of Vasic (2000). Minimization of Φ_S with respect to the four parameters was accomplished using the simplex-based routine fmins provided in the scientific computing package Matlab ("Using Matlab" 1998). The minimization process was straightforward, and converged quickly to the parameter values given in Table 1. Two important points regarding these parameters have been observed:

1) For a given aspect ratio, the optimal model

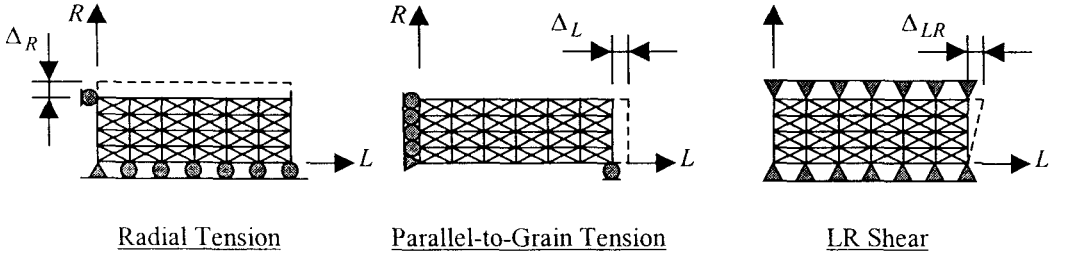

FIG. 4. Enforced displacements and boundary conditions.

TABLE 1. *Optimal model parameters for various levels of discretization.*

Mesh refinement ($L \times R$)	θ (radians)	k_L* (N/mm)	k_R* (N/mm)	k_D* (N/mm)
9 × 6	0.344	2,410	849	492
15 × 10	0.328	2,560	893	487
21 × 14	0.315	2,620	923	485

* These values are per mm of model width

parameters remain relatively independent of the cell size for a given value of a and l. This is an extremely useful result, as it implies that adjustments to cell geometry required by meshing constraints and model geometry can be efficiently accommodated by small adjustments to member stiffnesses.

2) The cell aspect ratio has a significant effect on the predicted parameters, and aspect ratios other than the assumed value of 2.0 will yield different values for θ, k_L, k_R, and k_D. Good results were achieved for aspect ratios of 1.0 and 3.0. However, once the aspect ratio exceeded a value of about 3, the rate of convergence of the minimization process slowed significantly.

CALIBRATION OF THE MODEL

Overview of test procedures and results for spruce subjected to radial tension

The complete load-deformation response of wood specimens loaded in tension perpendicular to the grain was measured by Vasic (2000). These experiments, aimed at evaluating the nonlinear softening response of eastern Canadian spruce, provide a strong basis for calibration of the lattice model in that particular loading case. The experimental setup, illustrated in Fig. 5, was designed to facilitate observation of stable post-peak strain-softening response. Specimens were glued to steel blocks that were then mounted in a steel load-sharing arrangement. The load-sharing arrangement was able to produce stable crack growth in the wood specimens. The load was applied to the steel beam above the specimen. The load on the wood specimen was determined by subtracting the load produced by the beam without a specimen from the measured load with the specimen. Deformation was determined from clip gages mounted on either side of the specimen. The tests were run in displacement control at a crosshead rate of 1 mm/min. This rate was chosen to obtain complete failure in 3–5 min.

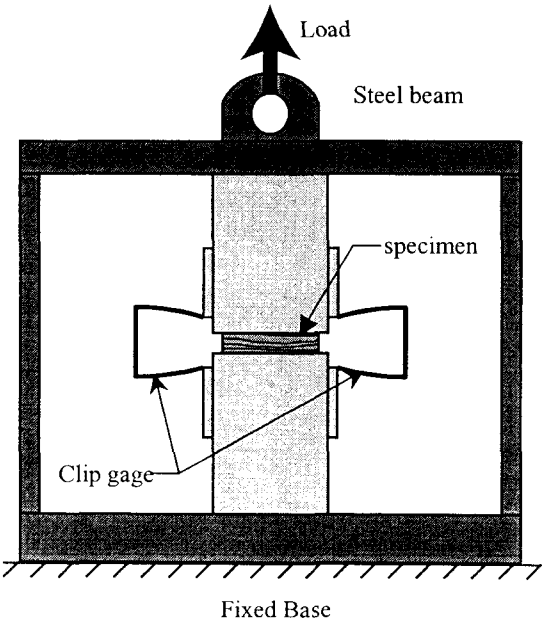

FIG. 5. Schematic of radial tensile tests.

The spruce specimens tested in radial perpendicular-to-grain tension were 4 mm thick, and ranged in size from 10 mm × 10 mm to 14 mm × 14 mm in the LT plane. Figure 6 shows the measured load-displacement results that have been normalized to a specimen size of 12 mm × 12 mm. Additional details of the testing program and results can be found in Vasic (2000).

Target response for lattice model

Application of the lattice model to the prediction of the observed small-specimen response in radial tension perpendicular-to-grain requires that a single target experimental load-displacement curve be determined. To achieve this, each experimental load-displacement curve shown in Fig. 6 was first smoothed us-

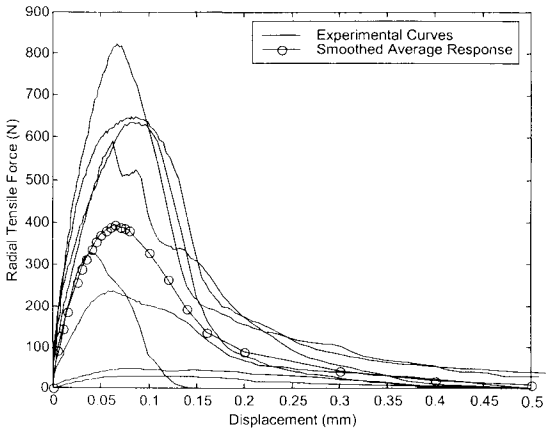

FIG. 6. Measured small-specimen radial tension perpendicular-to-grain behavior (Vasic 2000).

ing a moving average to allow easy interpolation. Second, the loads for all specimens were normalized to values corresponding to a 12-mm × 12-mm × 4-mm ($L \times T \times R$) specimen. This normalization was necessary since the tests were conducted on specimens ranging in size from 10 mm × 10 mm × 4 mm to 14 mm by 14 mm × 4 mm. Finally, 24 discrete displacements were selected at which the smoothed, normalized loads for all experiments were averaged. In addition to the six normalized experimental curves, Fig. 6 also shows this average curve, which was taken as the target response for the lattice model for radial tension perpendicular-to-grain. The mean radial tensile strength is 396 N, which corresponds to a stress of 2.75 MPa on a 12-mm × 12-mm specimen area. This value was 14.6% higher than the average perpendicular-to-grain tensile strength of 2.4 MPa reported in the Wood Handbook (1999) for red spruce at 12% moisture content.

The lattice model should also be able to predict *LR* shear response, which is primarily governed by the strength and stiffness of the diagonal members, and parallel-to-grain (*L*-direction) tension response. Determining the target load-displacement response for *LR* shear and parallel-to-grain tension was a challenging task. To the best of the authors' knowledge, load-displacement curves determined from tests on small specimens that describe the post-peak softening response of red spruce in tension parallel-to-grain and *LR* shear parallel-to-grain are not available. The nominal specimen response under these loading states was assumed to be linearly elastic until the failure load was reached.

The failure load for *LR*-shear was estimated as 1470 N. This value was computed by increasing the average shear strength of red spruce of 8.9 MPa (Wood Handbook 1999) by 14.6% and multiplying by a specimen area of 12 mm × 12 mm. While the Wood Handbook (1999) does not report a value for *L*-direction tensile strength of red spruce, its average modulus of rupture (MOR) is 74 MPa. This value was adjusted downward by 8.8% based on the reported *L*-direction tensile strength and MOR of Sitka spruce of 59.3 MPa and 65 MPa, respectively, and then adjusted up by 14.6% based on observed radial tension strength. The failure load for a specimen with an area of 4 mm × 12 mm in *L*-direction tension was then computed as 3710 N.

Calibration procedure

Prediction of the progressive damage and softening observed in the small-specimen radial tension perpendicular-to-grain tests requires the determination of the strengths and coefficients of variation of the individual members of the lattice model. A 15 × 10 ($L \times R$) lattice model was used to determine strength and stiffness parameters. The effect of mesh refinement is considered later in this section. The following nine independent member strength and stiffness parameters can be adjusted to match experimental and nominal response: the mean strength of each member type ($\bar{P}_L$, $\bar{P}_R$, and $\bar{P}_D$), the coefficient of variation in strength of each member type (COV_{P_L}, COV_{P_R}, and COV_{P_D}), and the coefficient of variation of stiffness of each member type (COV_{k_L}, COV_{k_R}, and COV_{k_D}). The mean member stiffnesses ($\bar{k}_L$, $\bar{k}_R$, and $\bar{k}_D$) were fixed for all analysis at the values determined by

fitting the elastic constants as described previously.

Preliminary analyses indicated that considering all nine parameters to be independent was computationally impractical; in addition, existing data do not provide guidance on appropriate magnitudes of the coefficients of variation. To overcome these difficulties, the number of parameters was reduced to six by assuming that $COV_{P_L} = COV_{k_L} = COV_L$, $COV_{P_D} = COV_{k_D} = COV_D$, and $COV_{k_R} = COV_{P_R} = COV_R$. Initial attempts at simultaneously fitting radial tension perpendicular-to-grain, *LR* shear, and parallel-to-grain tension response by allowing all six parameters to vary were unsuccessful. Therefore, the parameters providing a best fit to the data in a least squares sense were determined with the three-phase process described as follows.

Parameter estimation for LR shear response.—First, the response of the lattice in *LR* shear parallel-to-grain was analyzed. This loading was chosen for initial examination because the *LR* shear stiffness and strength are governed almost exclusively by the stiffness and strength of the diagonal elements. The values of COV_D and $\bar{P}_D$ were determined to provide the best fit to the shear response by minimizing the following objective function, ϕ_{LR}:

$$\Phi_{LR}(\bar{P}_D, COV_D) = \left[\left(\frac{(S_{1/2} - S^*_{1/2})}{S_{1/2}}\right)^2 + \left(\frac{(S_{max} - S^*_{max})}{S_{max}}\right)^2\right]^{1/2} \quad (3)$$

In Eq. (3), S^*_{max} is the model-predicted peak shear force and $S^*_{1/2}$ is the model-predicted shear force at half the displacement corresponding to S^*_{max}. These values were both taken as the average of 20 simulations, where properties of each diagonal member were generated for each simulation assuming a normal distribution of strength and stiffness. Similarly, S_{max} is the expected shear failure load of 1470 N and $S_{1/2}$ is the expected shear force at half the displacement corresponding to the expected shear failure load. This objective function was purposely constructed to ensure that its minimization resulted in a good fit to both the shear modulus and the ultimate shear strength, which are the two constitutive parameters readily available in the literature. An initial starting value of 100 N for $\bar{P}_D$ was estimated from the average member force in each diagonal element when a shear force of S_{max} was applied to a linearly elastic lattice model. The starting value for COV_D was taken as 0.20. The values of COV_L and COV_R were fixed at 0, and the values of $\bar{P}_L$ and $\bar{P}_R$ were assigned artificially large values to prevent failure of the parallel-to-grain and radial perpendicular-to-grain members. We emphasize that these members have very little effect on *LR* shear response. These initial parameter values yielded $\phi_{LR} = 0.15$. The minimum value of ϕ_{LR} was 0.08, which corresponds to $\bar{P}_D = 80$ N and $COV_D = 0.15$.

Parameter estimation for response in radial tension perpendicular-to-grain.—The target radial tension response described previously and shown in Fig. 6 was used to determine the values of COV_R and $\bar{P}_R$. The objective function for radial tension response, ϕ_R, was taken as follows, where T_i is the experimental smoothed average load at the ith radial displacement Δ_i (see Fig. 6), and T^*_i is the force predicted by the lattice model at the ith radial displacement.

$$\Phi_R(\bar{P}_R, COV_R) = \left[\sum_{i=1}^{24} ((T_i - T^*_i)/T_i)^2\right]^{1/2} \quad (4)$$

Including the point (0, 0), there are 24 points defining the smoothed average response curve. In the determination of ϕ_R, the values of $\bar{P}_D$ and COV_D were held at the previously determined optimal values of 80 N and 0.15, respectively. We note that this objective function differs significantly from that used for *LR*-shear (Eq. 3) and that used for *L*-direction tension (presented in the following section). This is due to the fact that for radial tension, detailed experimental data were available that fully describe the nonlinear, softening response. If such data were available in *LR*-

TABLE 2. *Values of Φ_R for $40 \le \bar{P}_R \le 50$ and $0.25 \le COV_R \le 0.50$.*

P_R	COV_R					
	0.25	0.30	0.35	0.40	0.45	0.50
40 N	2.10	2.33	2.14	2.45	2.29	1.95
42 N	2.14	1.58	2.01	2.10	2.13	1.89
44 N	2.04	1.83	2.05	2.09	2.21	1.72
46 N	1.87	1.93	1.77	1.62	1.78	1.84
48 N	2.17	1.74	1.49	2.04	1.92	1.68
50 N	2.15	1.97	1.99	1.78	1.81	1.54

shear and *L*-direction tension, objective functions similar to Eq. (4) could be constructed for all loading conditions.

Reasonable values of $\bar{P}_R$ and COV_R were estimated by manually varying their values and observing response. This initial step yielded the following likely range of parameter values: $40 \le \bar{P}_R \le 50$ and $0.25 \le \text{COV}_R \le 0.50$, for which values of ϕ_R were then calculated. To ensure a smooth variation in ϕ_R, each force T_i^* was determined for each pair of parameters as the average of 20 independent simulations using randomly generated member properties. Table 2 gives the values of ϕ_R corresponding to this range of parameter values. The minimum value of ϕ_R corresponded to $\bar{P}_R = 48$ N and $\text{COV}_R = 0.35$.

Parameter estimation for parallel-to-grain tension response.—The values of $\bar{P}_L$ and COV_L were determined to provide the best fit to the parallel-to-grain tension response by minimizing the following objective function, ϕ_L:

$$\Phi_L(\bar{P}_L, \text{COV}_L) = \left[\left(\frac{(Q_{1/2} - Q_{1/2}^*)}{Q_{1/2}}\right)^2 + \left(\frac{(Q_{\max} - Q_{\max}^*)}{Q_{\max}}\right)^2\right]^{1/2} \quad (5)$$

This objective function was constructed based on the same philosophy as ϕ_{LR} in an attempt to match both the elastic modulus and the ultimate tensile strength parallel-to-grain. In Eq. (5), $Q_{\max}^*$ is the maximum model-predicted tension force, and $Q_{1/2}^*$ is the model-predicted parallel-to-grain tension force at half the displacement corresponding to $Q_{\max}^*$. These values were both taken as the average of 20 simulations, where properties of each *L*-direction member were randomly generated for each simulation assuming a normal distribution of strength and stiffness. Similarly, $Q_{\max}$ is the expected tensile failure load of 3410 N, and $Q_{1/2}$ is the tension force at half the displacement corresponding to $Q_{\max}$. A starting value of 600 N for $\bar{P}_L$ was estimated from a few initial simulations, and the initial value for COV_L was taken as 0.20. The values of $\bar{P}_R$, $\bar{P}_D$, COV_R and COV_D were fixed at the previously determined optimal values. The optimal values for $\bar{P}_L$ and COV_L were 700 N and 0.20, respectively, at $\phi_L = 0.02$.

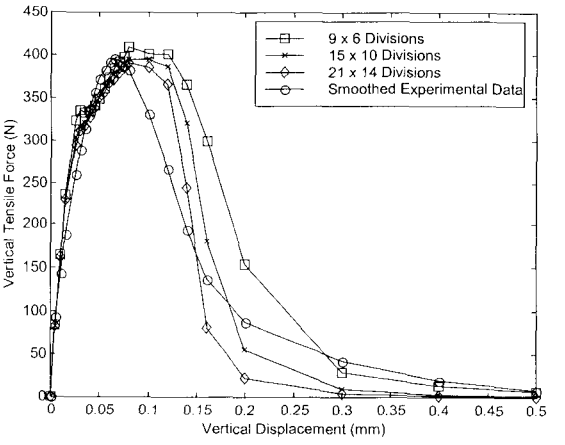

FIG. 7. Predicted and experimental radial tensile perpendicular-to-grain behavior.

MODEL PREDICTIONS AND SIGNIFICANCE OF RESULTS

Using the previously determined optimal parameters, responses of a 12-mm × 12-mm × 4-mm specimen to the loading conditions of radial perpendicular-to-grain tension, parallel-to-grain tension, and *LR* shear were simulated. Each of the responses was computed as the average of 100 independent simulations with randomly generated material properties. Figures 7–9 show the model load-displacement response and the target response for the three loading conditions. The primary stress

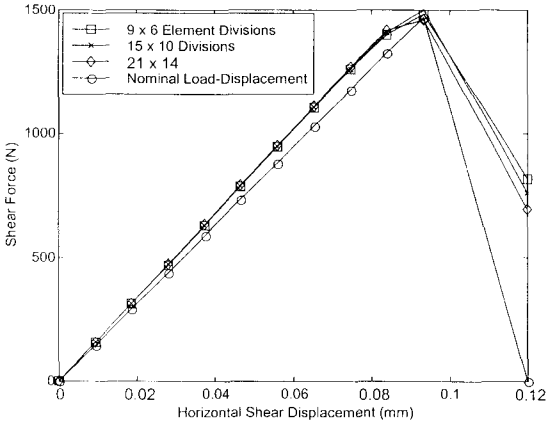

FIG. 8. Predicted and nominal *LR* shear parallel-to-grain behavior.

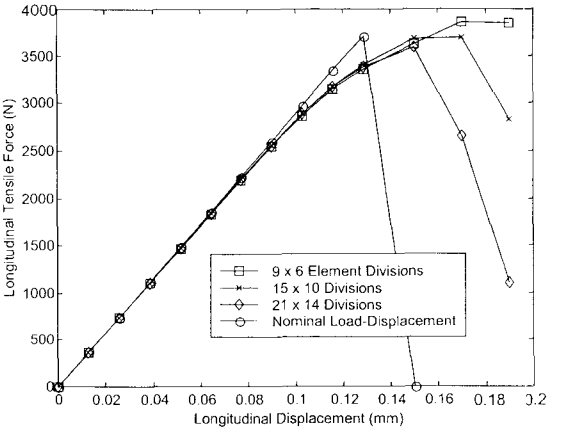

FIG. 9. Predicted and nominal tension parallel-to-grain behavior.

state of interest was radial tension perpendicular-to-grain, and the model fit to the mean experimental data was considered good (Fig. 7). In addition, the fit to the nominal shear response was considered good. The predicted post-peak response in parallel-to-grain tension was not as good as that achieved for radial tension and *LR*-direction shear, although both the stiffness and the magnitude of the peak load are accurately predicted by the lattice model. This is discussed in more detail later in this section.

We note that while the nominal load-displacement response in both *LR* shear and *L*-direction tension (Figs. 8 and 9) was taken as nearly brittle fracture, the post-peak capacity and strain softening that has been observed for radial tension may exist for *LR* shear and *L*-direction tension. However, the authors are not aware of any small-scale data that illustrate this behavior.

In addition to the base level of discretization with 15 × 10 element divisions, simulations using models with 9 × 6 element divisions and 21 × 14 element divisions were conducted in an attempt to assess the effects of finite element mesh refinement. The mean strengths of the members in the model with 9 × 6 members were determined by scaling $\bar{P}_R$, $\bar{P}_D$, and $\bar{P}_L$ by the ratio of (15 + 1)/(9 + 1) = 1.6, which corresponds to the ratio of the number of elements in the R-direction for the base 15 × 10 element mesh and the 9 × 6 element mesh. Similarly, the mean member strengths for the model with 21 × 14 elements were scaled by the ratio (15 + 1)/(21 + 1) = 0.73. We note that these scale factors are not ideal for all loading states, since both the radial perpendicular-to-grain tension response and parallel-to-grain tension response also depend on the diagonal elements, whose mean strength should be scaled by 15/9 and 15/21 for the 9 × 6 and 21 × 14 element meshes, respectively.

This simple scaling procedure produced good results for LR shear (Fig. 8). For the loading state of radial tension perpendicular-to-grain, the maximum load of 396 N is overpredicted by about 1% when 9 × 6 element divisions are employed. The model with 21 × 14 elements also gives acceptable results, under-predicting the maximum load by only 2%. However, the shape of the predicted radial tension load-displacement curve varies at different levels of mesh refinement, with increasing levels of mesh refinement better capturing the sharp descending branch. For parallel-to-grain tension, the peak load is less accurately predicted for all levels of mesh refinement, and the steepness of the descending branch increases rapidly with increasing levels of mesh refinement. Overall, it is concluded that this

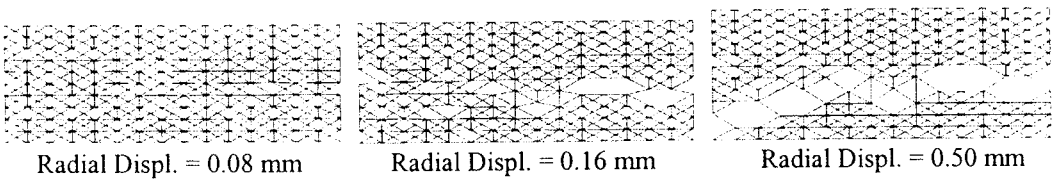

(a) Lattice Model Predictions

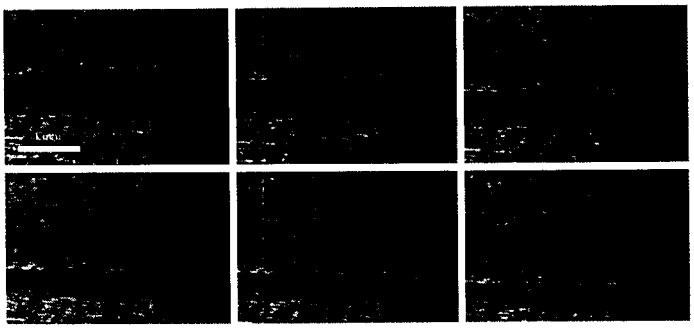

(b) Experimentally Observed Crack Growth and Bridging

FIG. 10. Damage evolution in specimen subjected to radial tension perpendicular-to-grain.

simple scaling gives reasonable results; however the topic of mesh refinement certainly warrants further study.

Figure 10a shows the lattice model members (that remain intact) at different magnitudes of perpendicular-to-grain radial tensile displacement, illustrating the predicted evolution of damage. The initial damage occurring at low displacement magnitudes is widely dispersed throughout the specimen. As displacements increase, individual fracture planes merge, eventually resulting in a tortuous fracture path that eventually travels as a major crack through the full member width along the grain. This model-predicted response is consistent with the crack bridging phenomenon observed in small-specimen wood fracture in spruce shown in Fig. 10b (Vasic et al. 2001; Vasic and Smith 1996). This crack bridging has not been successfully captured with conventional continuum-based linear or nonlinear elastic fracture mechanics approaches (Vasic 2000).

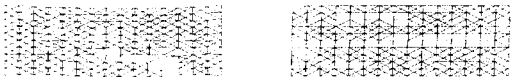

(a) Lattice Model Fracture Patterns for *L*-direction Tension and *LR* Shear

(b) Observed Small-specimen *L*-direction Tensile Fracture

FIG. 11. Damage evolution in specimen subjected to tension parallel-to-grain.

Figure 11a shows the remaining lattice model members after peak load has been reached for both *L*-direction tension and *LR* shear. In the case of *L*-direction tension, the damage is less localized since both the diagonal and *L*-direction members carry significant force. This results in a relatively tortuous fracture path, which is consistent with the fracture patterns seen in small-specimen tests of spruce-pine-fir specimens recently conducted at the University of Maine (Fig. 11b). However, for the case of *LR* shear, distinct fracture planes emerge in which almost all diagonal

members have failed. These observed fracture patterns explain why the lattice model predicts brittle fracture in *LR* shear, but not in *L*-direction tension.

Taken as a whole, the results of this work demonstrate several items of significance:

- *The lattice formulation can simultaneously capture elastic response, load-deformation behavior, and failure patterns in three different orientations of stress.* This is accomplished through a fairly simple model formulation with variable in element properties.
- *Model parameters can be estimated through a relatively straightforward optimization procedure, with elastic constants and strength properties as inputs.* To a large extent, the determination of optimal member properties can be accomplished independently for both elastic constants and strengths under simple stress states. However, it may be possible to develop more sophisticated schemes for parameter estimation where responses under several loading conditions are considered simultaneously.
- *Mesh refinement and length scale effects warrant further study.* Although reasonable predictions can be achieved for different levels of mesh refinement with a simple scaling of material properties, model response is sensitive to mesh refinement. Further research should address the effects of mesh refinement and the issue of length scale. This is extremely important, as ultimately the scale of the mesh should represent inherent length scales in wood macro- and mesostructure.

POTENTIAL FOR PRACTICAL IMPLEMENTATION

Explicit simulation of macrostructure and defects

The mechanical properties of wood are significantly affected by its growth ring structure, the presence of defects such as knots and spiral grain, and moisture content. We have only considered lattice models of small, clear-grained specimens, and it must be acknowledged that their lack of incorporation of growth ring structure and earlywood/latewood boundaries is a significant shortcoming. However, the lattice models are naturally suited to incorporating this feature, as cell size in the *R*-direction can be easily adjusted so the growth ring thickness is a multiple of this dimension. Further, the strength and stiffness of individual model elements can be based on whether they fall within an earlywood or latewood ring. This cell size will also allow future models to capture the disorder most relevant for structural applications, including grain deviation, shrinkage cracks, and spatial variation of properties due to varying moisture content. At length scales smaller than the growth ring, disorder can be represented by the statistical distribution of individual element properties. Micro- and mesoscale features can be incorporated into the lattice models as additional experimental data becomes available.

To illustrate the lattice model's potential ability to capture the effect of grain deviation, simulations were completed for a model with grain angles of 0°, 45°, and 90°. For simplicity, the model was assumed to be 12 mm × 12 mm in the *L* and *R* directions, and 12 mm thick. The simulations employed the same lattice cell geometry and element strength and stiffness properties of the previous models. The model boundaries were taken as fixed on the left face, and gradually increasing horizontal displacements were applied to the right face of the model as shown in Fig. 12.

The failure mode predicted by the simulations for a grain angle of 45° is essentially a shear failure that propagates inward from the model corners, and in the *L*-direction as shown in Fig. 12. This is consistent with failures observed in laboratory tests of specimens with significant grain deviations, which often fracture along a growth ring (Bodig and Jayne 1993). The failure mode was quite brittle, with a sudden drop in capacity at an enforced displacement of 0.7 mm.

It is well known that in addition to affecting failure mode, grain angle significantly reduces

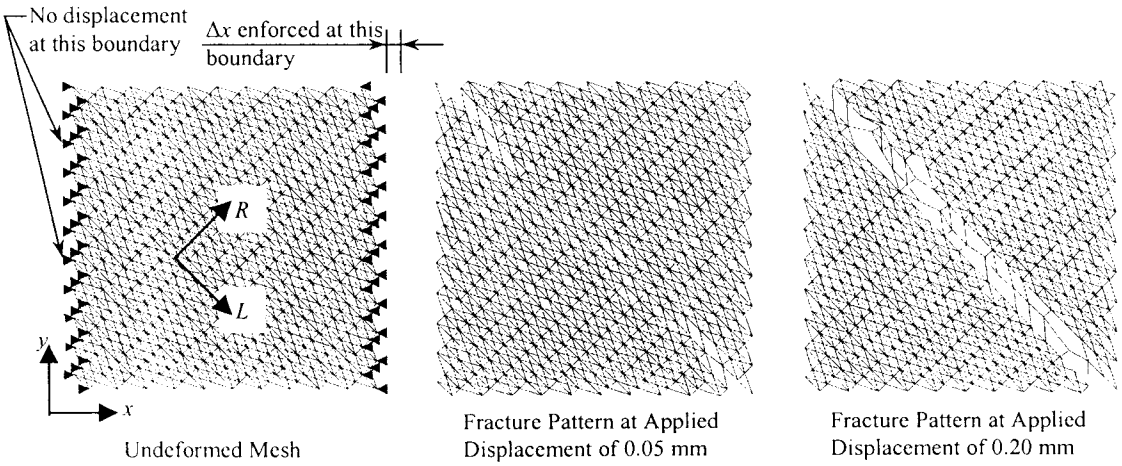

FIG. 12. Lattice with grain angle of 45°.

tensile capacity. The peak loads predicted by the model—based on the average of 10 simulations—were 10,710 N, 1,113 N, and 407 N for grain angles of 0°, 45°, and 90°, respectively. One widely used formula for predicting the variation in strength with grain angle is Hankinson's formula (Hankinson 1921), which while originally developed for use with compressive failures has also been applied for tensile failures such as those considered here (Cowin 1979). It is interesting to note that with the *L*- and *R*-direction capacities of this lattice model, Hankinson's formula predicts a tensile capacity of 784 N for a grain angle of 45°, which is 30% below that predicted by the lattice model. This overprediction of strength by the lattice model could be due at least in part to its lack of consideration of growth rings and the difference between earlywood and latewood strengths. Future research efforts on the use of lattice models to predict the structural response of wood should focus in better mimicking wood structure and explicit inclusion of defects.

Model size and computational requirements

It must be acknowledged that the lattice simulations of this study were performed for very small specimens, and the practical simulation of progressive fracture and failure of structural members such as beams, columns, or connections using lattice models of this study would require significant computational resources. This is especially true in light of material variability and the need for Monte-Carlo simulations.

However, as with any finite-element based simulation, solution speed is primarily governed by the efficiency of the algorithm used to solve the system stiffness equations. Several investigators working with discrete lattice models of concrete have tackled this problem. Jirásek and Bažant (1995) utilized a technique where the effect of stiffness degradation with progressive fracture was captured through the application of external inelastic forces, which made explicit updating of the system stiffness matrix unnecessary. Schlangen and Garboczi (1996) addressed this issue through the use of an iterative, conjugate-gradient solver; however, they did not perform preconditioning, which can significantly reduce computational expense. With appropriate preconditioners, the conjugate-gradient method has been shown to be extremely powerful for solving both linear and nonlinear finite-element problems in structural mechanics (Davids and Turkiyyah 1999).

Another approach that would significantly decrease computational requirements would be the adoption of a "local-global" modeling

approach, where a relatively coarse continuum finite-element model is used in regions of low stress (where the assumptions of orthotropic elasticity are reasonable) to maximize efficiency. The continuum could be explicitly coupled with lattice models near defects and in regions where significant nonlinearity and/or fracture is expected. Because the progressive failure and fracture in the lattice model will affect the kinematics of the entire member, the continuum and lattice would need to be meshed together using elements with compatible shape functions at the continuum/lattice boundary.

SUMMARY AND CONCLUSIONS

A lattice model consisting of longitudinal, radial, and diagonal elements was proposed to simulate the response of clear wood to three simple loading cases. A least squares minimization procedure was used to fit the spring constants of the lattice elements to the four bulk elastic constants in two dimensions. Mean strengths and coefficients of variation for the lattice elements were determined with a least squares minimization using experimentally obtained load-deformation curves for radial tension and published strength values for shear and tension parallel-to-grain. The lattice model accurately predicted peak load and the experimentally observed post-peak strain softening in perpendicular-to-grain tension. However, the post-peak shape of the load-deformation curve was affected by the degree of mesh refinement. Damage localization in radial tension can be observed with the lattice model, including crack bridging and microcracking around the critical crack. The lattice model successfully modeled parallel-to-grain shear response, which proved to be relatively insensitive to mesh refinement. However, strength and post-peak response were not as accurately predicted for parallel-to-grain tension response, and this loading case was particularly sensitive to mesh refinement. Details regarding the practical implementation of the lattice models were also discussed, including explicit incorporation of growth rings and defects (such as knots and grain deviations) and computational issues.

The methodology described in this paper may serve as a foundation for predicting structural behavior of wood and wood composite systems. However, there are several critical issues that must be addressed in future research:

- *Consideration of length scales and incorporate growth patterns and geometrical defects.* As discussed earlier, a natural length scale might be growth ring thickness. Morphology-based lattice models are ideally suited to model the observed strength and stiffness differentials between latewood and earlywood, and could also allow the treatment of common defects such as knots and sloping grain that often govern the strength of a structural member.
- *Validation of the model for pieces of wood of other sizes.* This is closely tied to the consideration of length scale and defects, as larger members are more likely to have strength-reducing defects.
- *Treatment of compression response.* The response of wood in compression is dramatically different than in tension, and this must be addressed. This will likely necessitate the formulation of new (and possibly ductile) compressive failure criteria for the individual lattice members.
- *Consideration of combined loading conditions.* The models considered in this paper individually examined simple loading conditions; actual structures often fail under complex combined loading conditions.
- *Extension of the lattice models to the prediction of three-dimensional response.* While some structures can be idealized as one- or two-dimensional, successful prediction of response in the presence of strength-reducing defects and combined loadings will require the use of three-dimensional models.

REFERENCES

AU, T., AND P. CHRISTIANO. 1993. Fundamentals of structural analysis. Prentice Hall, Inc., Englewood Cliffs, NJ.

BODIG, J., AND J. R. GOODMAN. 1973. Prediction of elastic parameters for wood. Wood Science 5(4):249–264.

———, AND B. JAYNE. 1993. Mechanics of wood and wood composites. Krieger Publishing Co., Malabar, FL.

COWIN, S. C. 1979. On the strength and anisotropy of bone and wood. Trans. ASME 46:832–838.

CRAMER, S. M., AND J. R. GOODMAN. 1983. Model for stress analysis and strength prediction of lumber. Wood Fiber Sci. 15:118–149.

———, AND ———. 1986. Failure modeling: A basis for the strength prediction of lumber. Wood Fiber Sci. 18: 446–459.

———, AND W. FORHELL. 1990. Method for simulating tension performance of lumber members. J. Struct. Eng. 116:2729–2746.

CURTIN, W., AND H. SCHER. 1990. Brittle fracture of disordered materials: A spring network model. J. Mater. Res. 5(3):535–553.

DAVIDS, W. G., AND G. M. TURKIYYAH. 1999. Multigrid preconditioner for unstructured nonlinear 3D FE models. J. Eng Mech. 125:186–196.

HANKINSON, R. L. 1921. Investigation of crushing strength of spruce at varying angles of grain. Air Service Information Circular No. 259, U.S. Air Service.

HIBBELER, R. C. 1990. Structural analysis. Macmillan Publishing Company, New York, NY.

ILLSTON, J. M., ed. 1994. Construction materials: Their nature and behaviour. E & FN Spon, London, UK.

JIRÁSEK, M., AND Z. BAŽANT. 1995. Macroscopic fracture characteristics of random particle systems. Int. J. Fracture 69:201–228.

RAGHUPRASAD, B., D. BHAT, D., AND G. BHATTACHARYA. 1998. Simulation of fracture in a quasi-brittle material in direct tension—a lattice model. Eng. Fracture Mech. 61:445–460.

SCHLANGEN, E., AND E. GARBOCZI. 1996. New method for simulating fracture using an elastically uniform random geometry lattice. Int. J. Eng. Science 34(10):1131–1144.

———, AND ———. 1997. Fracture simulations of concrete using lattice models: computational aspects. Eng. Fracture Mech. 57(2/3):319–332.

"USING MATLAB." The Mathworks, Inc., Natick, MA, 1998.

VASIC, S. 2000. Applications of fracture mechanics to wood. Ph.D. thesis, University of New Brunswick, Fredericton, Canada.

———, AND I. SMITH. 1996. The brittleness of wood in tension perpendicular to the grain: Micromechanical aspects. Pages 818–820. *In* Proc. World Conf. Timber Engineering, COST 508, Stuttgart, Germany.

———, ———, AND E. LANDIS. 2001. Fracture zone characterization—Micro-mechanical study. Wood Fiber Sci. (in press).

WOOD HANDBOOK. Forest Products Laboratory Report No. FPL-GTR-113. Madison, WI, 1999.